Correlative Analysis of Genetic Alterations and Everolimus Benefit in Hormone Receptor-Positive, HER2-Negative Advanced Breast Cancer: Results From BOLERO-2

Hortobagyi, et al

ONLINE-ONLY SUPPLEMENTAL MATERIAL

Correlative Analysis of Genetic Alterations and Everolimus Benefit in Hormone Receptor-Positive, HER2-Negative Advanced Breast Cancer: Results From BOLERO-2

Prof. Gabriel N. Hortobagyi, MD[1]; David Chen, PhD[2]; Prof. Martine Piccart, MD[3]; Prof. Hope S. Rugo, MD[4]; Howard A. Burris III, MD[5]; Prof. Kathleen I. Pritchard, MD[6]; Prof. Mario Campone, MD[7]; Prof. Shinzaburo Noguchi, MD[8]; Alejandra T. Perez, MD[9]; Ines Deleu, MD[10]; Mikhail Shtivelband, MD[11]; Norikazu Masuda, MD[12]; Shaker Dakhil, MD[13]; Ian Anderson, MD[14]; Douglas M. Robinson, PhD[15]; Wei He, PhD[15]; Abhishek Garg, PhD[15]; E. Robert McDonald III, PhD[15]; Hans Bitter, PhD[15]; Alan Huang, PhD[15]; Tetiana Taran, MD[2]; Thomas Bachelot, MD[16]; Fabienne Lebrun, MD[3]; David Lebwohl, MD[2]; José Baselga, MD[17]

[1]Department of Breast Medical Oncology, The University of Texas MD Anderson Cancer Center, 1515 Holcombe Blvd, Unit 1354, Houston, TX 77030, USA; [2]Oncology Global Development, Novartis Pharmaceuticals Corporation, One Health Plaza, East Hanover, NJ 07936, USA; [3]Jules Bordet Cancer Institute, Université Libre de Bruxelles, Medicine Department 1, Boulevard de Waterloo 125, B-1000 Brussels, Belgium; [4]University of California, San Francisco, Helen Diller Family Comprehensive Cancer Center, 1600 Divisadero Ave, Second Floor, Box 1710, San Francisco, CA 94115, USA; [5]Sarah Cannon Research Institute, Drug Development, 3322 West End Ave, Suite 900, Nashville, TN 37203, USA; [6]Sunnybrook Odette Cancer Centre and the University of Toronto, 2075 Bayview Avenue, T2, Toronto, ON, Canada M4N 3M5; [7]CLCC René Gauducheau, Centre de Recherche en Cancerologie, Nantes-Saint-Herblain, France; [8]Department of Breast and Endocrine Surgery, Osaka University Medical School, 2-2-E10 Yamadaoka Suita, Osaka 565-0871, Japan; [9]Memorial Cancer Institute, Breast Cancer Program, 3700 Johnson St, Hollywood, FL 33021, USA; [10]The Louis Meesterstraat 5, 9100 Sint-Nikolaas, Belgium; [11]Ironwood Cancer & Research Centers, 685 S Dobson Rd, Chandler, AZ 85224, USA; [12]Department of Surgery, Breast Oncology, NHO Osaka National Hospital, 2-1-14 Hoenzaka, Chuou-ku, Osaka-city 540-0006, Japan; [13]Cancer Center of Kansas, 818 N Emporia Ste 403, Wichita, KS 67214, USA; [14]Redwood Regional Oncology Center, 3555 Round Barn Circle, Santa Rosa, CA 95403, USA; [15]Novartis Institutes for BioMedical Research, Inc., 250 Massachusetts Ave, Cambridge, MA 02139, USA; [16]Centre Léon Bérard, 28 rue Laënnec, 69008 Lyon, France; [17]Memorial Sloan-Kettering Cancer Center, 1275 York Avenue – Suite M2015, New York, NY 10065, USA

METHODS

Identification of Genetic Alterations

Tumor DNA was extracted from 40-μm thickness of formalin-fixed, paraffin-embedded (FFPE) tissue sections, which had been histologically confirmed to contain predominantly tumor tissue. Two hundred ng was used for library construction and hybrid capture. Among a total of 302 samples from which evaluable next-generation sequencing (NGS) data were obtained, about 80% were analyzed by sequencing the exons of a panel of 182 cancer-related genes and the rest by an expanded panel containing 236 genes (Supplemental Table 2). Deep sequencing of the exons of prespecified cancer-related genes was conducted using Illumina HiSeq2000 at Foundation Medicine Inc. (Cambridge, MA).[1] Samples with a minimum unique coverage of 250× were included in the subsequent analysis. Nucleotide sequence alterations were identified by comparison against the corresponding National Center for Biotechnology Information (NCBI) reference sequence, and then queried against known alterations in the Catalogue of Somatic Mutations in Cancer (COSMIC; available at http://cancer.sanger.ac.uk/cancergenome/projects/cosmic/) and in the Single Nucleotide Polymorphism Database (dbSNP; available at http://www.ncbi.nlm.nih.gov/snp/). Non-synonymous sequence alterations recorded in COSMIC but not in dbSNP were designated as known somatic mutations, those recorded in dbSNP were designated as germline mutations, and those with no match in either COSMIC or dbSNP were designated as novel mutations. In addition, copy number variations were assessed,

including amplifications (defined as genes with copy number ≥6 copies) and bi-allelic deletions.

The numbers of somatic mutations and the types of alteration are shown in Supplemental Fig 2. In summary, after filtering out known germline mutations, 1,572 missense mutations, 197 nonsense and frameshift mutations, and 136 splice variants, and small insertions and deletions were identified. Among them, 473 were known somatic variations. The remaining 1,432 were novel sequence variations not previously described.

Filtering for germline mutations using public databases such as dbSNP tends to include germline mutations that have high population frequency, but may not rule out novel or rare/unique germline mutations in the patients. To estimate the fraction of germline changes among the novel mutations, we sequenced 71 germline DNA samples (23.5% of NGS population) with matching tumor samples. Among the novel mutations detected in these 71 tumor samples, 65% were found to be germline mutations. On the other hand, only five (4%) known mutations (ie, mutations present in COSMIC but not in dbSNP) from tumor samples were also found in the matching germline samples. Based on these results, novel short-variant mutations (ie, SNVs and INDELs) were not included in our analysis as the majority of these mutations are likely to be of germline origin. All copy number variations, both known and novel, were included in the correlative analyses.

mTOR and *FGFR2* Mutations

Mutations reported in the *mTOR* gene were mostly novel (ie, not reported in either dbSNP or COSMIC databases). Only four mutations—namely H640R, I2500N, D1224Y, and P2141L—were confirmed somatic mutations (ie, not found in their matching germline DNA samples among the 71 samples sequenced). The remaining six mutations (R1905S, R1482C, A949P, A1134V, Y1974H, and R1482H) were present in the tumor samples for which germline DNA samples were not sequenced, and therefore cannot be reliably classified into germline or somatic mutations. Of these 10 mutations, four were present in the kinase or FAT domains, where mutations often result in higher mTOR activity.[2] Three of these four patients received everolimus and had a longer PFS (8.2–19.4 months) than the median PFS (7.0 months) of the everolimus arm in the NGS cohort (Supplemental Fig 3A). In addition, one everolimus-treated patient whose PFS was 14.1 months had a confirmed somatic mutation (H640R near the N-terminus of the HEAT domain), which potentially could disrupt the interaction between mTOR and Raptor.[3] However, PFS benefits from everolimus were variable in the patients with mutations in other mTOR domains (Supplemental Fig 3A).

The genetic alterations detected in *FGFR2* were more diverse and included missense and nonsense mutations, gene amplifications, and rearrangements. Of the nine patients with unequivocal genetic alterations, one patient had a genomic rearrangement leading to a truncation in the C-terminal region with no clear evidence of FGFR2 hyperactivity (because of an intact kinase domain),[4] five patients had copy-number amplification, and three patients had point mutations (a known N549K mutation, a nonsense Y769* mutation, and a novel T32A mutation). Excluding the two patients

with genetic alterations of no clear gain of function effect (ie, *FGFR2* rearrangement with noncoding DNA at the C-terminal region, and a novel T32A mutation), the median PFS of remaining seven patients was only 2.7 months (range, 1.3–3.9 months), significantly shorter than the 7.0-month median PFS for everolimus-treated patients in the NGS population. These seven patients all had at least one additional known oncogenic alteration in *PIK3CA*, *CDK4*, *CDKN2A/2B*, *IGF1R*, *KDR*, or *Myc* (Supplemental Fig 2). We also detected N549K mutations in two patient samples (one in each treatment arm), with very low mutation allele frequency of only 2%, suggesting that these tumors are heterogeneous, with the vast majority of their cells having wild-type *FGFR2*. Interestingly, the everolimus-treated patient whose PFS was 14.1 months also had a confirmed somatic mutation in *mTOR* and in *PIK3CA* exon 9.

TCGA HR$^+$, HER2$^-$ Breast Cancer Cohort

The HR$^+$, HER2$^-$ breast cancer subpopulation of 477 patients was selected from The Cancer Genome Atlas network (TCGA) complete breast cancer cohort based on the immunohistochemistry (IHC) and fluorescence in situ hybridization (FISH) status of hormone (progesterone and estrogen) receptors and HER2.[5] For comparing mutation frequencies in TCGA HR$^+$, HER2$^-$ breast cancer cohort against the BOLERO-2 NGS population, we included the somatic short-variants (non-synonymous missense, nonsense, INDELs, and frame-shift mutations), and copy-number aberrations as reported using GISTIC scores in TCGA.[6] Because copy-number variants in the BOLERO-2 NGS population only comprised bi-allelic loss and copy-number variants of high-level amplifications (≥6 copies), we only included the copy-number variants with

GISTIC scores –2 (corresponding to bi-allelic loss) and +2 (corresponding to high-level amplification) for the TCGA cohort.

For CIN-score calculations on the TCGA cohort, raw gene-level copy-number values instead of GISTIC scores were used. All the genetic alteration data for TCGA samples were downloaded from cBioPortal using the R-package *cgdsr* (http://cran.r-project.org/web/packages/cgdsr).

CIN Metric for Scoring Chromosomal Instability: Establishment on BOLERO-2 Data and Validation on TCGA Data

For each tumor sample from the BOLERO-2 NGS cohort, genes were first sorted according to their genomic location. The number of switches or breakpoint events, as represented by genomic rearrangements and copy-number mismatches between neighboring genes on each chromosome, was then calculated. The magnitude of copy-number changes was summarized by summing the absolute difference in copy numbers between neighboring genes on each chromosome. The number of switches and magnitude of switches across all the samples in the cohort were then ranked separately, and the sum of the ranks was used to define the chromosomal instability metric (CIN) for each sample in the cohort (Supplemental Fig 1).

We established the robustness of the CIN score for estimating chromosomal instability using a targeted gene panel by evaluating the CIN score on 477 HR^+, $HER2^-$ breast cancer samples in TCGA for which the whole-exome copy-number calls were available. The CIN scores were calculated for TCGA samples using the same method as described in Supplemental Fig 1. We calculated CIN scores using the raw copy-

number data for all the genes covered in the whole-exome TCGA data, or a subset of genes comparable in number with the targeted cancer gene panel used in the NGS assay on samples from BOLERO-2. For the CIN scores calculated using a random set of genes (Supplemental Fig 4), the numbers of genes similar to those present on the targeted panel were drawn randomly from the genes covered by the whole-exome TCGA data, and CIN scores were calculated for each sample using these random sets of genes. All analyses comparing random gene sets with targeted panel or whole-exome were performed on at least 100 different random gene sets.

While all the genes present on our targeted gene panel have biologic significance in cancer, we found that CIN calculations using random gene sets (CIN^{Rand}) provide an equally good estimate of chromosomal instability (with an average correlation coefficient of 0.95 between CIN^{Panel} and CIN^{Rand}, Supplemental Fig 6). Furthermore, the comparison of the targeted gene panel CIN scores to CIN calculated from whole-exome data shows a very high correlation between the two (correlation coefficient of 0.96 for CIN^{Panel} vs CIN^{WE}, and correlation coefficient of 0.92-0.98 for CIN^{Rand} vs CIN^{WE}). These two datasets demonstrate that, although the whole-genome and transcriptome assays are presently preferred methods for measuring chromosomal instability, developing an equally valid scoring metric using data acquired from a medium-sized pan-cancer gene panel such as ours provides a beneficial expansion of the utility of the NGS data increasingly collected in oncology practice.

PTEN Immunohistochemistry Assay

Tissue slides were stained with hematoxylin and eosin (H&E) and evaluated for the presence of tumor. PTEN expression was assessed by immunohistochemistry using clone 138G6 antibody (Cell Signaling Technology, Danvers, MA). Both the staining intensity (0, 1+, 2+, and 3+) and the percentage of positive tumor cells at each intensity and cellular location (cytoplasm) were evaluated and reported as Histo-scores.

Analysis of AKT and pS6 Activation in Cell Lines

Reverse Phase Protein Array (RPPA) analyses of phospho-AKT (Serine 473) and phopsho-S6 (Serine 240/244) were conducted in 422 cancer cell lines of various lineages at the RPPA Core Facility at MD Anderson Cancer Center according to standard procedure.[7] The RPPA expression levels were Z-score transformed. Alteration of the *PIK3CA* gene was determined as part of the Cancer Cell Line Encyclopedia (CCLE) project.[8]

Statistical Analyses

Known genetic alterations were summarized using descriptive statistics. Progression-free survival (PFS) for patients whose tumors harbored altered versus wild-type status for the indicated gene was compared using Kaplan-Meier estimates. In addition, for individual genes, the Cox proportional hazards model was used to compute the hazard ratio for PFS and its associated 95% confidence interval. For assessments of each gene or combinations of genes within a specific signaling pathway, PFS comparisons were made using a Cox model adjusted for clinical covariates that were significantly

imbalanced between treatment arms and varied by comparison. The covariates (prior chemotherapy, Eastern Cooperative Oncology Group (ECOG) status, age, and race) were checked between the two treatment arms of each biomarker-defined subpopulation.

SUPPLEMENTAL TABLES

Supplemental Table 1. Median PFS and HR at Different CIN Score Cut-offs. CIN Score Cut-off of 75th Percentile and Higher Show No Benefit of Everolimus in CIN High Subgroup as Compared to CIN Low Subgroup.

Cut point	Group		N	Events	Median PFS (95% CI)	HR (95% CI)
25%	CIN Low	PBO.low	30	25	4.21 (2.53–6.93)	0.49 (0.29–0.82)
		RAD.low	57	35	8.41 (5.13–11.07)	
	CIN High	PBO.high	63	53	2.79 (1.51–4.17)	0.41 (0.29–0.58)
		RAD.high	152	92	6.93 (5.78–8.05)	
50%	CIN Low	PBO.low	49	41	4.14 (2.63–5.55)	0.42 (0.28–0.63)
		RAD.low	104	59	8.48 (6.8–11.07)	
	CIN High	PBO.high	44	37	2.79 (1.45–4.17)	0.44 (0.29–0.66)
		RAD.high	105	68	6.83 (5.55–7.13)	
60%	CIN Low	PBO.low	55	46	4.11 (2.53–5.49)	0.43 (0.3–0.63)
		RAD.low	127	74	8.31 (6.8–10.87)	
	CIN High	PBO.high	38	32	2.79 (1.48–4.21)	0.43 (0.28–0.68)
		RAD.high	82	53	6.77 (5.49–7.13)	
65%	CIN Low	PBO.low	59	49	4.11 (2.63–5.42)	0.41 (0.28–0.59)
		RAD.low	137	76	8.48 (6.93–11.1)	
	CIN High	PBO.high	34	29	2.79 (1.45–4.37)	0.5 (0.31–0.79)
		RAD.high	72	51	5.59 (4.44–6.9)	
70%	CIN Low	PBO.low	65	55	2.86 (2.63–5.26)	0.39 (0.28–0.55)
		RAD.low	146	81	8.41 (6.93–11.07)	
	CIN High	PBO.high	28	23	4.14 (1.45–5.52)	0.57 (0.34–0.95)
		RAD.high	63	46	5.78 (4.53–6.93)	
75%	CIN Low	PBO.low	71	60	2.86 (2.63–5.26)	0.39 (0.28–0.54)
		RAD.low	155	86	8.41 (6.93–11.07)	
	CIN High	PBO.high	22	18	4.14 (1.41–5.52)	0.62 (0.35–1.08)
		RAD.high	54	41	5.59 (4.11–6.83)	

Supplemental Table 1. Median PFS and HR at Different CIN Score Cut-offs. CIN Score Cut-off of 75th Percentile and Higher Show No Benefit of Everolimus in CIN High Subgroup as Compared to CIN Low Subgroup.						
Cut point	**Group**		**N**	**Events**	**Median PFS (95% CI)**	**HR (95% CI)**
80%	CIN Low	PBO.low	76	64	4.01 (2.63–5.26)	0.42 (0.3–0.57)
		RAD.low	165	94	8.25 (6.8–10.87)	
	CIN High	PBO.high	17	14	4.14 (1.18–4.37)	0.49 (0.26–0.94)
		RAD.high	44	33	6.7 (4.53–7.03)	
85%	CIN Low	PBO.low	81	69	2.86 (2.63–4.21)	0.41 (0.3–0.56)
		RAD.low	175	98	8.25 (6.8–10.87)	
	CIN High	PBO.high	12	9	4.17 (0.92–8.94)	0.56 (0.26–1.21)
		RAD.high	34	29	6.7 (4.53–7.03)	

Supplemental Table 2. Panel of Evaluated Cancer-Related Genes								
ABL1	CDK6	FGFR1	MAP2K4	PIK3CA	TSC2	STAT3	FANCE	MYCL1
AKT1	CDK8	FGFR2	MCL1	PIK3CG	VHL	TBX22	FANCF	MYD88
AKT2	CDKN2A	FGFR3	MDM2	PIK3R1	WT1	TNKS	FANCG	NFE2L2
AKT3	CDKN2B	FGFR4	MDM4	PRKDC	ABL2	TNKS2	FANCL	NFKBIA
ALK	CDKN2C	FLT1	MEN1	PTCH1	BCL2A1	USP9X	FGF10	NOTCH2
APC	CEBPA	FLT3	MET	PTEN	BCL2L1	ARID2	FGF14	NUP93
AR	CHEK1	FLT4	MITF	PTPN11	BCR	ASXL1	FGF19	PALB2
ARAF	CHEK2	GATA1	MLH1	RAF1	CDH2	ATRX	FGF23	PBRM1
ARFRP1	CRKL	GNA11	KMT2A	RARA	CDH20	AXL	FGF3	PDK1
ARID1A	CRLF2	GNAQ	MPL	RB1	CDH5	BARD1	FGF4	PIK3R2
ATM	CTNNB1	GNAS	MRE11A	RET	EPHA6	BCOR	FGF6	PPP2R1A
ATR	DDR2	GPR124	MSH2	RICTOR	EPHA7	BCORL1	FOXL2	PRDM1
AURKA	DNMT3A	HRAS	MSH6	RPTOR	EPHB4	BLM	GATA2	PRKAR1A
AURKB	DOT1L	IDH1	MTOR	RUNX1	EPHB6	BRIP1	GATA3	RAD50
BAP1	EGFR	IDH2	MUTYH	SMAD2	ERCC2	BTK	GID4	RAD51
BCL2	EPHA3	IGF1R	MYC	SMAD4	FOXP4	CBFB	GNA13	RNF43
BCL2L2	EPHA5	IKBKE	MYCL	SMARCA4	GUCY1A2	CDC73	GRIN2A	ROS1
BCL6	EPHB1	IKZF1	MYCN	SMARCB1	HOXA3	CDK12	GSK3B	SETD2
BRAF	ERBB2	INHBA	NF1	SMO	HSP90AA1	CDKN1B	HGF	SF3B1
BRCA1	ERBB3	IRS2	NF2	SOX10	IGF2R	CIC	IL7R	SOCS1

Supplemental Table 2. Panel of Evaluated Cancer-Related Genes								
BRCA2	ERBB4	JAK1	NKX2-1	SOX2	INSR	CREBBP	IRF4	SPEN
CARD11	ERG	JAK2	NOTCH1	SRC	LRP6	CSF1R	KAT6A	SPOP
CBL	ESR1	JAK3	NPM1	STK11	LTK	CTCF	KDM5A	STAG2
CCND1	ETV1	JUN	NRAS	SUFU	MLL	CTNNA1	KDM5C	STAT4
CCND2	ETV4	KDM6A	NTRK1	TET2	MYCL1	DAXX	KEAP1	TNFRSF14
CCND3	ETV5	KDR	NTRK2	TGFBR2	PHLPP2	EMSY	KLHL6	TSHR
CCNE1	ETV6	KIT	NTRK3	TMPRSS2	PKHD1	EP300	MAP3K1	WISP3
CD79A	EWSR1	KRAS	PAK3	TNFAIP3	PLCG1	FAM123B	MED12	XPO1
CD79B	EZH2	LRP1B	PAX5	TOP1	PTCH2	FAM46C	MEF2B	ZNF217
CDH1	FANCA	MAP2K1	PDGFRA	TP53	PTPRD	FANCC	MLL	ZNF703
CDK4	FBXW7	MAP2K2	PDGFRB	TSC1	SMAD3	FANCD2	MLL2	

Gene names in **Red** are only present on the 182-gene panel.
Gene names in **Blue** are only present on the updated 236-gene panel.
Gene names in black were common to both the gene panels (and were included in the current analysis).

Supplemental Table 3. Concordance of Samples With Mutations in p53 Pathway Genes (*TP53*, *MDM2*, and *MDM4*) by CIN Subgroups		
	p53 Pathway (*TP53*, *MDM2*, and *MDM4* genes)	
CIN	Mutated	Wild-Type
High	57	19
Low	60	166
Likelihood of p53 pathway mutation (high vs low CIN): Odds ratio = 8.23 (95% CI, 4.41–5.92); *P* = 1.423e-13 (Fisher's exact test).		

Supplemental Table 4. PFS by Treatment Arm in Patient Subsets Categorized by Alterations in Key Genetic Pathways						
	Description	Group	n	PFS Events	Median PFS, mo (95%CI)	Hazard Ratio (95%CI)
PIK3CA, *FGFR1/2*, and *CCND1* variations	Mutation in ≤1 genes (*PIK3CA, FGFR1/2, CCND1*)	PBO.Sing.≤1 EVE.Sing.≤1	66 161	55 94	4.1 (2.7–5.6) 8.1 (6.8–10.2)	0.44 (0.32–0.62)
	Mutation in ≥2 genes (*PIK3CA, FGFR1/2, CCND1*)	PBO.Mult.≥2 EVE.Mult.≥2	27 48	23 33	2.8 (1.4–4.2) 5.6 (3.9–6.9)	0.44 (0.25–0.77)
P53 pathway variations	Wild-type *TP53*, *MDM2*, and *MDM4* genes	PBO.WT EVE.WT	54 133	45 74	4.0 (2.6–6.8) 8.1 (6.8–10.9)	0.43 (0.30–0.63)
	Mutation in *TP53*, *MDM2*, or *MDM4* genes	PBO.ALT EVE.ALT	39 76	33 53	2.9 (1.5–4.2) 6.8 (5.2–8.5)	0.45 (0.29–0.70)
Abbreviations: ALT, alteration; CI, confidence interval; EVE, everolimus; Mult, multiple (ie, alteration in ≥2 relevant genes); PBO, placebo; PFS, progression-free survival; Sing, single (ie, alteration in ≤1 relevant gene); WT, wild-type.						

REFERENCES

1. Frampton GM, Fichtenholtz A, Otto GA, et al: Development and validation of a clinical cancer genomic profiling test based on massively parallel DNA sequencing. Nat Biotechnol 31:1023-31, 2013

2. Grabiner BC, Nardi V, Birsoy K, et al: A diverse array of cancer-associated MTOR mutations are hyperactivating and can predict rapamycin sensitivity. Cancer Discov 4:554-63, 2014

3. Knutson BA: Insights into the domain and repeat architecture of target of rapamycin. J Struct Biol 170:354-63, 2010

4. Wu YM, Su F, Kalyana-Sundaram S, et al: Identification of targetable FGFR gene fusions in diverse cancers. Cancer Discov 3:636-47, 2013

5. Cancer Genome Atlas Network: Comprehensive molecular portraits of human breast tumours. Nature 490:61-70, 2012

6. Beroukhim R, Getz G, Nghiemphu L, et al: Assessing the significance of chromosomal aberrations in cancer: methodology and application to glioma. Proc Natl Acad Sci U S A 104:20007-12, 2007

7. Tibes R, Qiu Y, Lu Y, et al: Reverse phase protein array: validation of a novel proteomic technology and utility for analysis of primary leukemia specimens and hematopoietic stem cells. Mol Cancer Ther 5:2512-21, 2006

8. Barretina J, Caponigro G, Stransky N, et al: The Cancer Cell Line Encyclopedia enables predictive modelling of anticancer drug sensitivity. Nature 483:603-7, 2012

SUPPLEMENTAL FIGURES

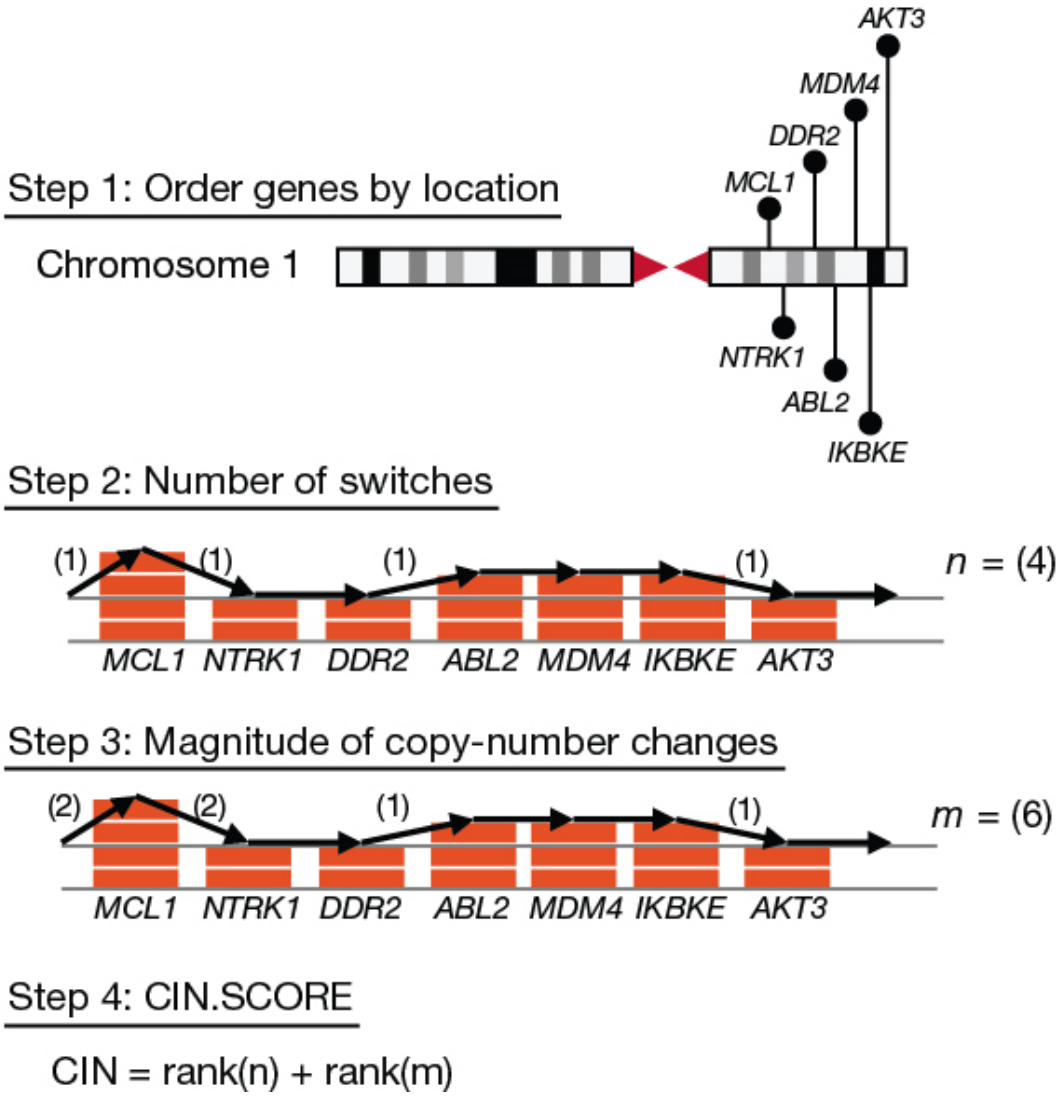

Supplemental Fig 1. CIN score calculation based on copy-number and genomic arrangements. *n*, number of copy-number switches/rearrangements; *m*, magnitude of copy-number changes.

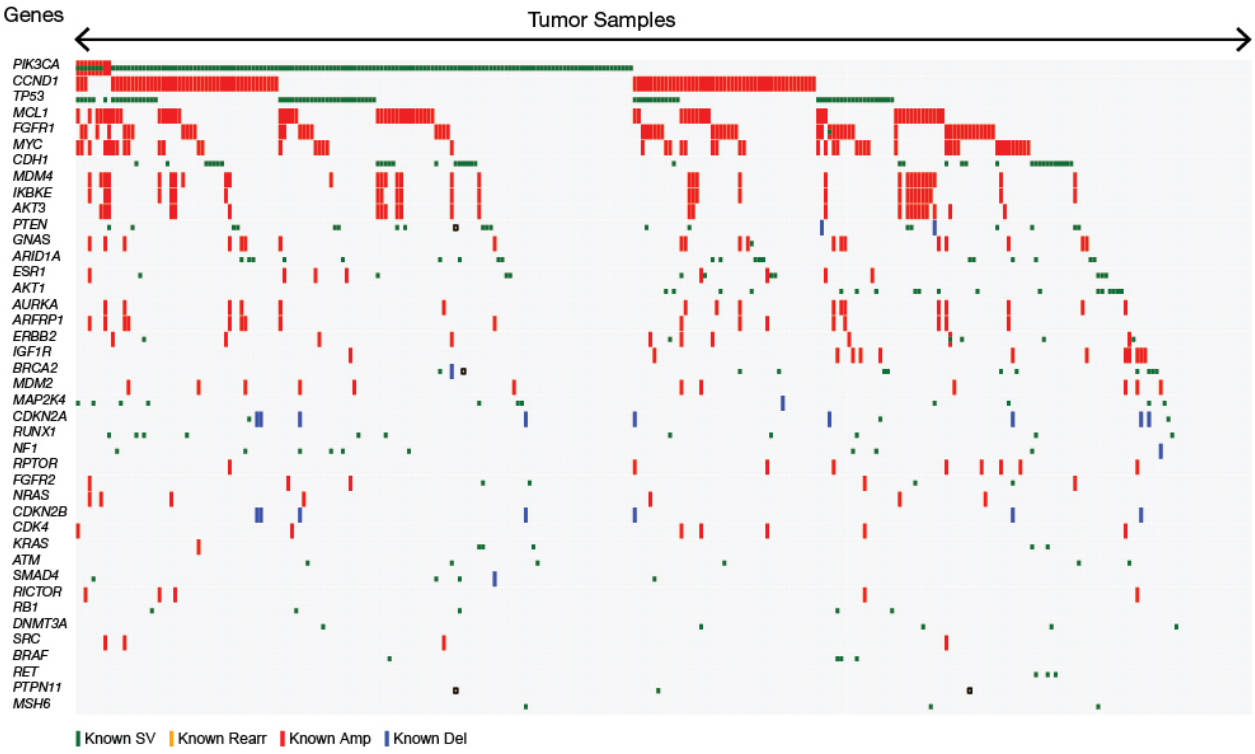

Supplemental Fig 2. Genetic alterations observed in patient tumors. Known amplifications (Amp), deletions (Del), rearrangements (Rearr) and somatic variations (SV) are shown. The 40 most frequently altered genes are included in the display above.

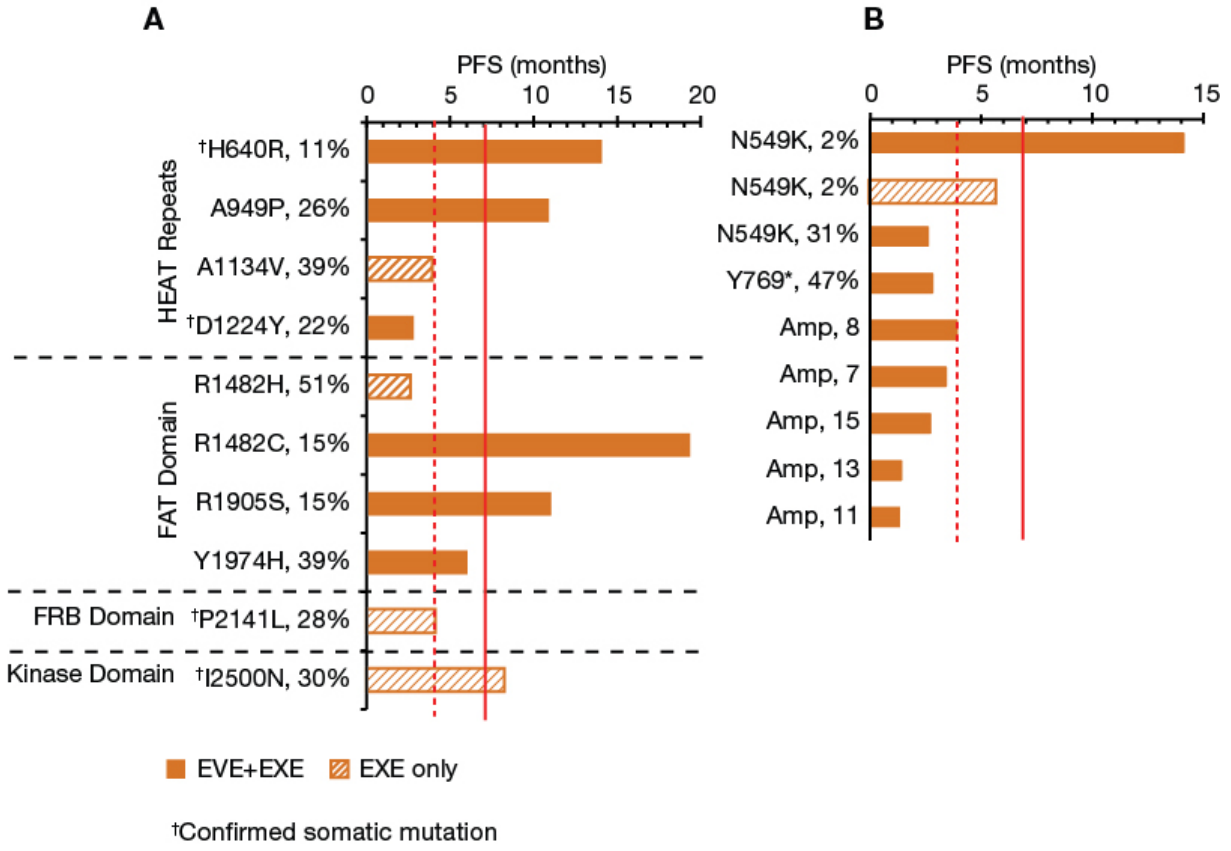

Supplemental Fig 3. Mutations reported in (A) *mTOR* and (B) *FGFR2* in the BOLERO-2 next-generation sequencing (NGS) population. Mutations reported here are either confirmed somatic (daggers; where matching germline samples were sequenced), or potentially somatic (samples for which matching germline samples were not sequenced, and somatic status is reported based on COSMIC, dbSNP database, and other germline samples sequenced in this study; see Methods). The minor allelic fractions of the short-sequence variants are reported as percentage of total number of reads at that position. For copy-number amplifications in *FGFR2* (Amp), numbers of copies observed in the tumor samples are reported. Progression-free survival (PFS) is reported in months; dashed vertical line represents the median PFS in the placebo arm (~4 months; 95% CI, 2.6-4.2 months), and the solid vertical line represents the median PFS in the

treatment arm (~7 months; 95% CI, 6.7-8.5 months) for the NGS population. Abbreviations: EVE, everolimus; EXE, exemestane.

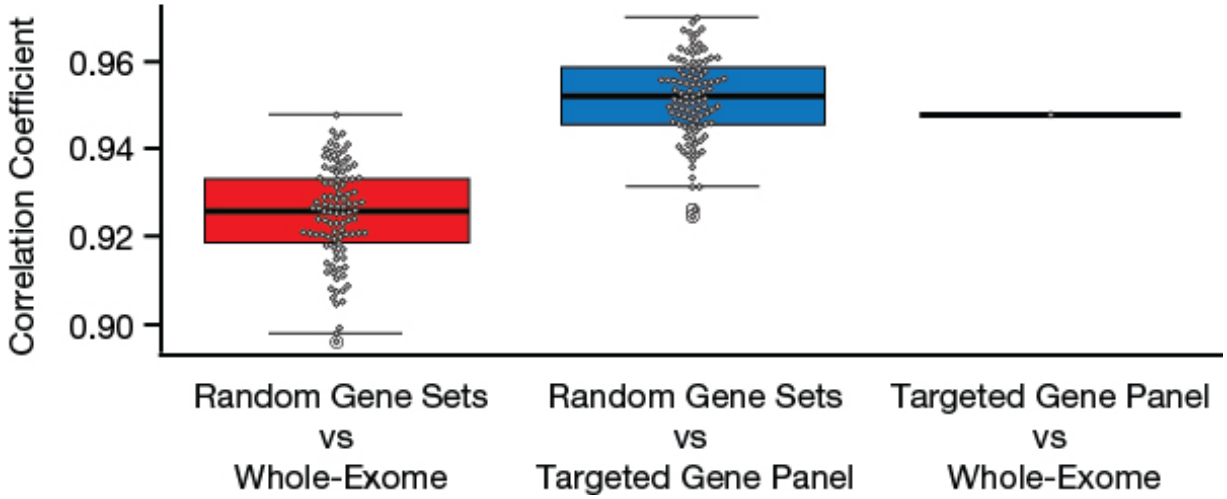

Supplemental Fig 4. CIN score: Whole-exome versus targeted panels on The Cancer Genome Atlas (TCGA) hormone receptor (estrogen and/or progesterone receptors)-positive, human epidermal growth factor receptor-2–negative cohort. For box-plots comparing random gene sets to whole-exome or the genes on our targeted panel (red and blue), 100 different simulations were performed with random gene sets. Pearson correlation was calculated between CIN scores from random gene sets and targeted-panel (blue) (or whole-exome [red]) on the TCGA samples. (See supplemental methods for additional details.)

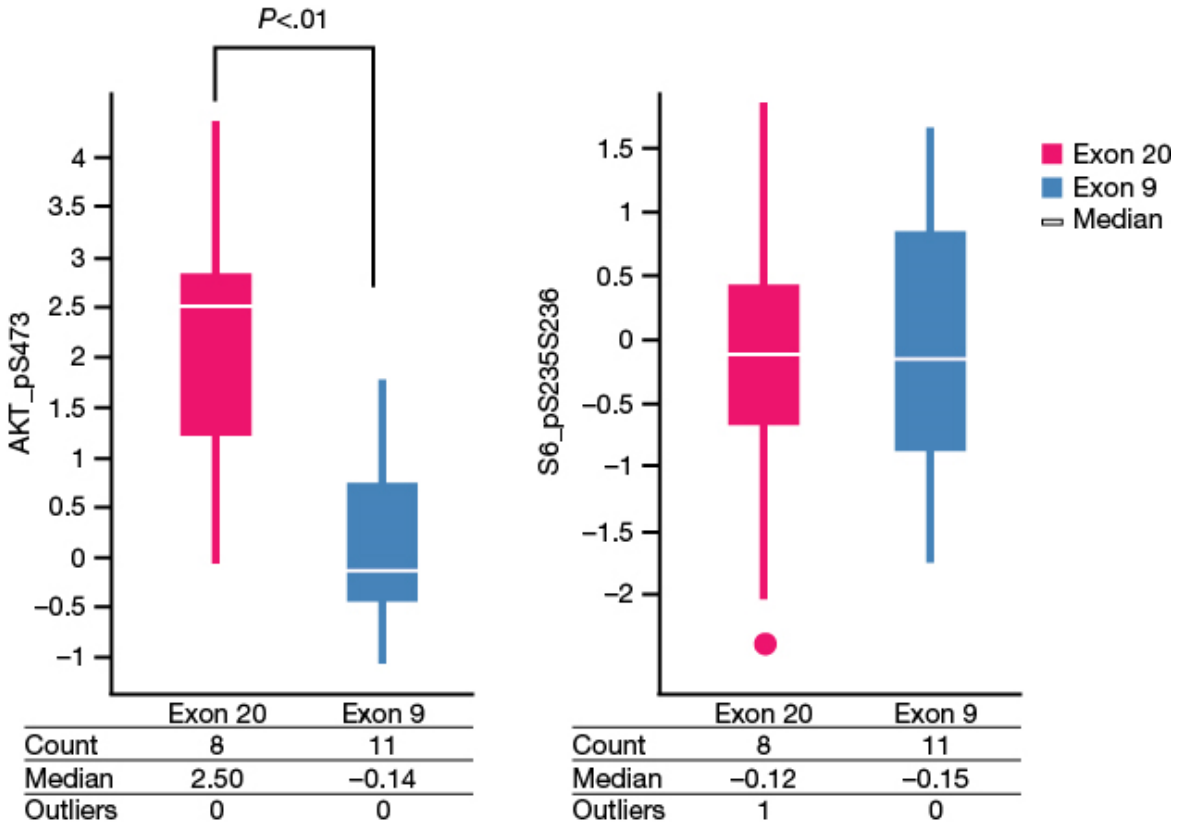

Supplemental Fig 5. Data from eight cell lines with *PIK3CA* exon 20 mutations and 11 cell lines with exon 9 mutations from Cancer Cell Line Encyclopedia (*PTEN* mutants were removed to avoid confounding factors) showed significantly higher phospho-AKT levels in those with exon 20 mutations versus exon 9 mutations, whereas their mammalian target of rapamycin (mTOR) activities (indicated by phospho-S6 level) were very similar.

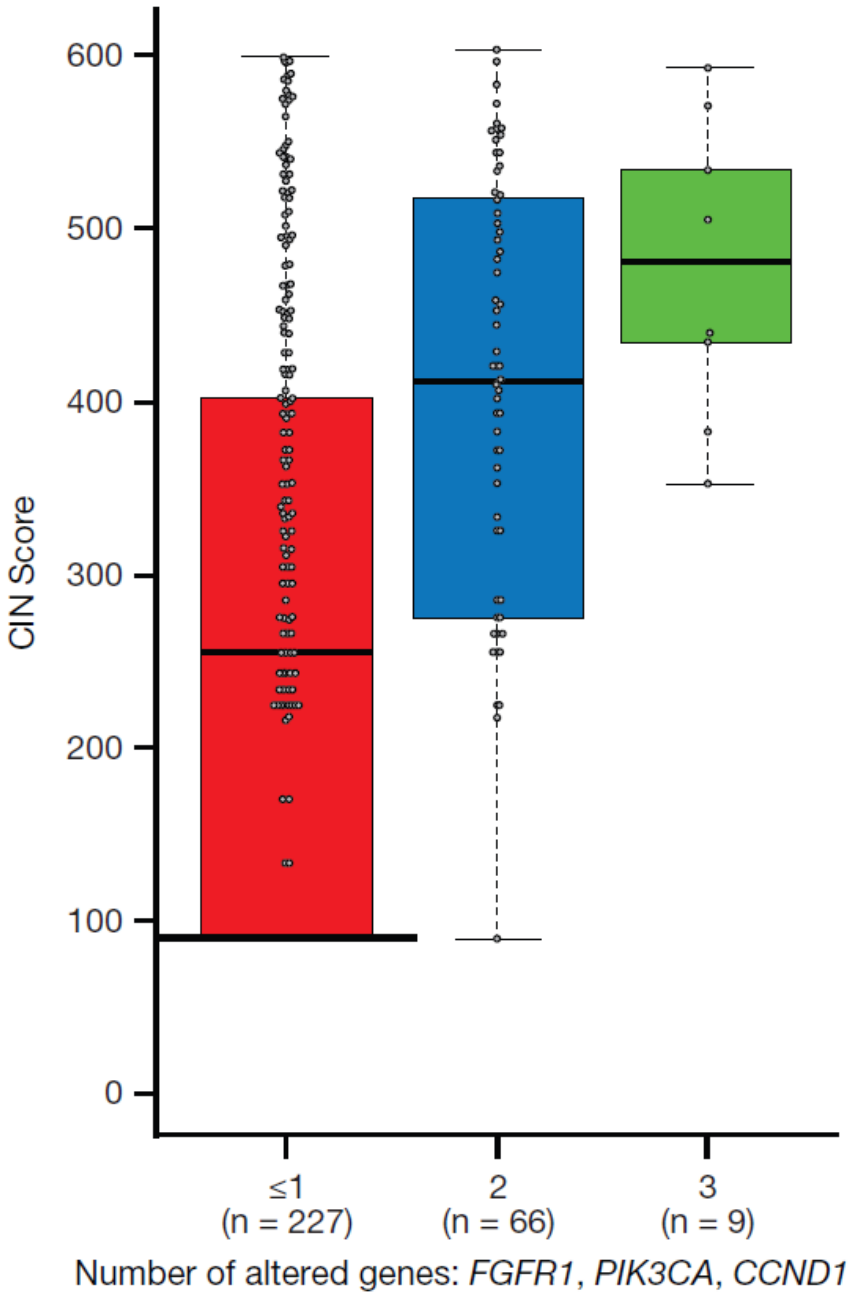

Supplemental Fig 6. Comparison of CIN score with number of mutations in these three frequently mutated genes (*FGFR1*, *PIK3CA*, and *CCND1*) shows the trend that samples with higher CIN score have higher number of mutations. However, the correlation is not perfect, as many samples with mutations in other genes can result in higher CIN scores.